Applied Mathematical Modelling 87 (2020) 180–202

Contents lists available at ScienceDirect

Applied Mathematical Modelling

journal homepage: www.elsevier.com/locate/apm

Theoretical model for variable helical angle of tensile armour wires in bent flexible pipes

Yang Zhou [a,b,*], Murilo Augusto Vaz [b], Xiaotian Li [b], Junpeng Liu [c]

[a] School of Mechatronic Engineering and Automation, Shanghai University, Shanghai, China
[b] Ocean Engineering Program, Federal University of Rio de Janeiro, Rio de Janeiro, Brazil
[c] College of Safety and Ocean Engineering, China University of Petroleum, Beijing, China

ARTICLE INFO

Article history:
Received 12 February 2020
Revised 22 April 2020
Accepted 1 June 2020
Available online 10 June 2020

Keywords:
Flexible pipes
Bending
Variable helical angle

ABSTRACT

This paper systematically addresses a theoretical model to account for the variation of the initial helical lay angle of the tensile armour wires in flexible pipes during bending condition. Based on differential geometrical discussion and curved beam theory, a non-linear differential equation system which contains the unknown variable helical angle is established. Moreover, different expressions of wires' strain before and after wires' slip are included in the paper to underline the discrepancy between scenarios in non-slippage and slippage regions. The variation of the armour wires helical angles, which are usually implicit in previous work, can be obtained numerically, revealing potential application in global bending problem. Case studies compared with results obtained through analytical and numerical models available in the literature as well as parametric analyses corresponding to original helical angle, initial tensile force, friction coefficient and bending curvature are performed to verify the feasibility of the proposed theoretical method.

1. Introduction

Flexible pipes are tubular composite structures which are now widely used in offshore oil and gas field, especially in deep water scenarios. The flexible pipe system represents an indispensable part, mainly designed for liquid and gas transportation. A typical structure of unbonded flexible pipe, as shown in Fig. 1, is composed of many reinforced independent layers with specific purposes that can suffer high global bending deformation.

Among the layers, tensile armours, conventionally made wound steel helical wires with a series of nearly rectangular cross-section, are the cardinal parts to provide low bending stiffness compared to axial and radial stiffness. Due to tensile loads and cycling bending, armour wires are also the primary cause for high cycle stress fatigue failure.

To date, extensive research focused on bending behavior of flexible pipes has been conducted in a way to investigate the local mechanical behavior of armour wires. Different approaches have been carried out in order to search for an optimized method to simulate and predict the structural response. Some studies [1–3] initially proposed theoretical methods to calculate stresses of armour wires based on Euler's formula. The bending stress of a helical wire on a bent cylinder can be derived by the simplified system under the assumption that only geodesic slip is allowed in the theoretical model. Moreover,

* Corresponding author at: School of Mechatronic Engineering and Automation, Shanghai University, Shanghai, China.
E-mail address: saber_mio@shu.edu.cn (Y. Zhou).

https://doi.org/10.1016/j.apm.2020.06.001
0307-904X/

Nomenclature

r	radius of the bent pipe
R	radius of the helical layer
θ, φ	angular coordinate
s	wire arclength
α	helical layer angle
ξ	variable helical angle, the complementary angle of α
$\boldsymbol{T}$	local unit tangential vector of the curve
$\boldsymbol{N}$	local unit normal vector of the surface
$\boldsymbol{B}$	local unit binormal vector
κ_g	geodesic curvature of the wire
κ_n	normal curvature of the wire
τ_g	torsion of the wire
$\boldsymbol{F}$, F	wire sectional force and its component in orthonormal basis
$\boldsymbol{M}$, M	wire sectional moment and its component
$\boldsymbol{p}$, p	wire distributed load and its component
$\boldsymbol{m}$, m	wire distributed moment and its component
κ	torus curvature $\frac{1}{R}$
E	elastic modulus
G	shear modulus
A	wire cross sectional area
ε	tangential strain of the wire
I_N	wire second N-axial moment of area
I_B	wire second B-axial moment of area
I_ρ	wire second polar moment of area
Δ_T, Δ_B	wire slips in $\boldsymbol{T}$ and $\boldsymbol{B}$ directions
Δ_c, Δ_p	wire slips in angular coordinate directions

Costello [4] developed a model for wire ropes considering curved beam equilibrium equations, contributing to the bending behavior study of flexible pipes.

Witz and Tan [5] derived an analytical model for helical layers of unbonded flexible pipes using energy method. In this model, the discussion of overall resultant bending moment was included. A hysteretic bending moment-curvature relationship was also proposed, reflecting the different observed behavior before and after armour wires' slip. Sævik [6] developed a 3D curved beam element by applying a computational model with prescribed curvature. Subsequently, the 3D curved element for umbilical analysis was improved by theoretical and experimental studies in [7–9]. In order to calculate stresses and slips in flexible armour layers, the bending behavior and local buckling resistance were investigated in [10,11]. Based on [11], Leroy and Estrier [12] improved the expressions of stresses and slips for both two armour layers. A repeated bending behavior with frictional effects was also analyzed in [12]. However, some geometrical assumptions such as the relation between torus coordinates θ and φ were made in the literature to support the structure of mathematical model.

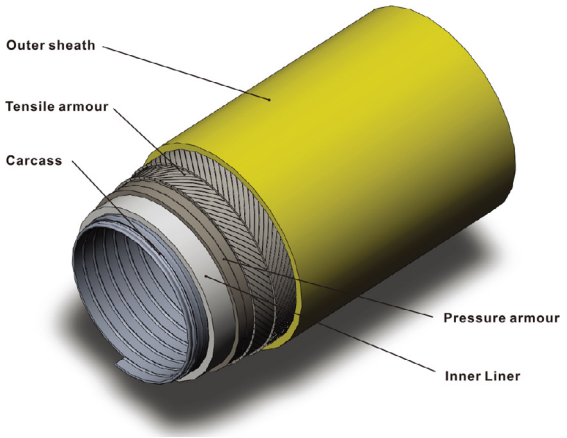

Fig. 1. The structure of flexible pipe.

Ramos and Pesce [13] also presented an analytical model incorporating bending, twisting and tension. The system can be solved assuming full-slip of the helical layers when subjected to bending. Brack et al. [14] studied the potential failure modes of flexible pipes subjected to combined forces by applying the finite element method. Another finite element model devoted to axisymmetric analyses was proposed by Bahtui et al. [15,16]. In the model, a fully explicit time-integration scheme was established. Østergaard et al. [17] focused on the geometrical configuration deriving and solving a unified system of differential equations and disregarding frictional effects. Based on [17], Østergaard et al. [18] then incorporated frictional forces and developed the cycling bending model under combined compression and bending. Moreover, bending behavior studies and the involved mechanics of flexible pipes were also investigated by both laboratory tests and three-dimensional finite element model in [19–23]. As a potential alternative in the field of oil/gas transportation in shallow water, Metallic Strip Flexible Pipes (MSFP) were further studied in [24,25] to underline the vital influence of tensile loads.

Although considerable research has been carried out through experimental and numerical approaches to analyze the mechanical behavior of armour wires in bent flexible pipes, few analytical models were established to determine the underlying mechanism of wires' slip mode under bending. In [12], slip of armour wires was divided into two orthogonal components represented the projections of real slip vector onto tangential and binormal directions, letting the armour wires move freely on the circular torus surface. Moreover, Zhou and Vaz [26] systematically analyzed the local mechanical behavior of armour wires based on the model provided in [12]. However, due to some unclear parts in the geometrical model, the original helical angle of armour wires was applied in this initial system. That is, although there are some established analytical models that describe the armour wires slip in bent flexible pipes, the changing of helical angle is fairly difficult to be calculated theoretically due to peculiar intrinsic characteristics of this differential geometry model. For instance, trying to establish the relations of traditional space between distance and angle in the case of non-Euclidean geometry is usually tough.

It is of great significance to study the underlying mechanism of variable helical angle of armour wires in bent flexible pipes. In global bending research of flexible pipes, there are several analytical models trying to simulate the hysteretic bending moment-curvature relation found in practical applications in offshore engineering. Witz and Tan [5] proposed that the hysteretic phenomenon was caused by the missing of part of bending stiffness after critical curvature during the bending process. Whereafter, Kebadze and other authors [27–29] put forward a new theoretical method that could explain the continuous change of bending stiffness. They introduced a smooth transition between non-slippage and slippage regions in moment-curvature function. The developed model still awaits verification on account of the constant bend stiffness hypothesis [30] corresponding to the curvature increase in the slippage region. In these analytical models, although helical angle has an important role to show influence on the final result of global bending stiffness, the original expression of bending moment itself can be only linear since the helical angle was considered as a constant. These analytical studies introduced nonlinear response based on different expressions in progressive and full slip regions due to frictional effect. If the problem based on variable helical angle of armour wires can be solved, an ameliorative arithmetic of this global bending problem which can better simulate the resultant moment will be established theoretically, i.e., the proposed method introduces nonlinearities in bending response solely related to the variable helical angle hypothesis.

This paper aims at investigating the mechanism of tensile armour wires in flexible pipes when helical angle is no longer considered as a constant under the bending condition. Based on existing theories in differential geometry and curved beam, an analytical approach is chosen to establish the non-linear differential equation system. Besides, differently from other discussions in the literature, the expressions of strains before and after wires' slip are separately introduced. From the equation system, the variation of the helical angle can be numerically calculated and the changing tendency of the armour wire angle is therefore clearly revealed.

2. Relevant geometry foundation

In this section, several basic mathematical foundations in differential geometry are listed. These fundamental equations are preliminaries for next geometrical discussion of local armour wires in flexible pipes. Since bent flexible pipes are tubular composite structures, it is essential to set up a mathematical description on curved surface structure.

A subset $\Sigma \subset \mathbb{R}^3$ is a regular surface, if it establishes a map, satisfying the following form,

$$\boldsymbol{\Sigma}(\boldsymbol{x}_\Sigma) : \mathbb{R}^2 \ni \boldsymbol{x}_\Sigma = \begin{bmatrix} \mu \\ \upsilon \end{bmatrix} \mapsto \boldsymbol{\Sigma}(\boldsymbol{x}_\Sigma) = \begin{bmatrix} x \\ y \\ z \end{bmatrix} \in \mathbb{R}^3 \tag{1}$$

The surface is continuous and smooth, namely, the vector form $\boldsymbol{\Sigma}(\boldsymbol{x}_\Sigma) = (x(\mu,\upsilon), y(\mu,\upsilon), z(\mu,\upsilon))$ can be used to study differential and integral calculus. All the geometrical quantities can be deduced from Eq. (1), including the first and second fundamental form, three local unit vectors (***T, N, B***) on the surface and two principal curvatures κ_1 and κ_2 which are the extreme values of normal curvature at one point. All the details and derivation are based on the theory of differential geometry by do Carmo [31].

If there exists an arbitrary curve s adhering to this surface, the normal vector of curve $\boldsymbol{n}$ is replaced by the normal vector of surface $\boldsymbol{N}$. Moreover, the tangential vectors $\boldsymbol{t}$ and $\boldsymbol{T}$ are coincident. Hence, a rotation from Frenet-Serret frame (***t, n, b***) to Darboux frame (***T, N, B***) is formulated, see Fig. 2. Note that, vectors $\boldsymbol{b}$ and $\boldsymbol{B}$ are not presented in the following figure for convenience. However, the two vectors can be easily obtained in corresponding frame by using the right-hand rule.

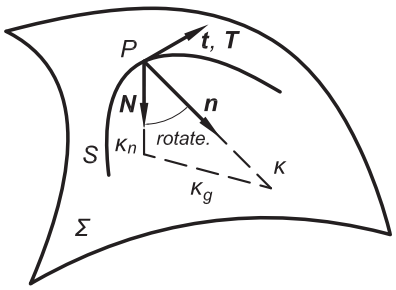

Fig. 2. Local frame transformation.

The unit normal vector $\boldsymbol{N}$ can be derived by the surface derivatives with respect to surface coordinates μ and υ, which span the tangent space on this curved surface.

$$\boldsymbol{N} = \frac{\frac{\partial \boldsymbol{\Sigma}}{\partial \mu} \times \frac{\partial \boldsymbol{\Sigma}}{\partial \upsilon}}{\left|\frac{\partial \boldsymbol{\Sigma}}{\partial \mu} \times \frac{\partial \boldsymbol{\Sigma}}{\partial \upsilon}\right|} = \frac{\boldsymbol{\Sigma}_\mu \times \boldsymbol{\Sigma}_\upsilon}{|\boldsymbol{\Sigma}_\mu \times \boldsymbol{\Sigma}_\upsilon|} \tag{2}$$

Let $\boldsymbol{t}_\mu$, $\boldsymbol{t}_\upsilon$ be the unit tangential vectors generated by two coordinates. Assuming ξ is the angle from $\boldsymbol{t}_\mu$ to $\boldsymbol{T}$, the unit tangential vector $\boldsymbol{T}$ will be given by,

$$\boldsymbol{T} = \cos\xi \cdot \boldsymbol{t}_\mu + \sin\xi \cdot \boldsymbol{t}_\upsilon = \cos\xi \frac{\boldsymbol{\Sigma}_\mu}{|\boldsymbol{\Sigma}_\mu|} + \sin\xi \frac{\boldsymbol{\Sigma}_\upsilon}{|\boldsymbol{\Sigma}_\upsilon|} \tag{3}$$

Hence the unit binormal vector is $\boldsymbol{B} = \boldsymbol{T} \times \boldsymbol{N}$.

The first fundamental form of a surface is defined as the following expression,

$$\begin{aligned} I &= (\mathrm{d}s)^2 = |\mathrm{d}\boldsymbol{\Sigma}|^2 = (\tfrac{\partial \boldsymbol{\Sigma}}{\partial \mu}\mathrm{d}\mu + \tfrac{\partial \boldsymbol{\Sigma}}{\partial \upsilon}\mathrm{d}\upsilon) \cdot (\tfrac{\partial \boldsymbol{\Sigma}}{\partial \mu}\mathrm{d}\mu + \tfrac{\partial \boldsymbol{\Sigma}}{\partial \upsilon}\mathrm{d}\upsilon) \\ &= \boldsymbol{\Sigma}_\mu \cdot \boldsymbol{\Sigma}_\mu (\mathrm{d}\mu)^2 + 2\boldsymbol{\Sigma}_\mu \cdot \boldsymbol{\Sigma}_\upsilon \mathrm{d}\mu\mathrm{d}\upsilon + \boldsymbol{\Sigma}_\upsilon \cdot \boldsymbol{\Sigma}_\upsilon (\mathrm{d}\upsilon)^2 \end{aligned} \tag{4}$$

The second fundamental form is then,

$$II = -\mathrm{d}\boldsymbol{\Sigma} \cdot \mathrm{d}\boldsymbol{N} = -(\tfrac{\partial \boldsymbol{\Sigma}}{\partial \mu}\mathrm{d}\mu + \tfrac{\partial \boldsymbol{\Sigma}}{\partial \upsilon}\mathrm{d}\upsilon) \cdot (\tfrac{\partial \boldsymbol{N}}{\partial \mu}\mathrm{d}\mu + \tfrac{\partial \boldsymbol{N}}{\partial \upsilon}\mathrm{d}\upsilon) \tag{5}$$

Since $\boldsymbol{\Sigma}_\mu \cdot \boldsymbol{N} = 0$, $\boldsymbol{\Sigma}_\upsilon \cdot \boldsymbol{N} = 0$,

$$\begin{aligned} \boldsymbol{\Sigma}_{\mu\mu} \cdot \boldsymbol{N} + \boldsymbol{\Sigma}_\mu \cdot \boldsymbol{N}_\mu = 0 \qquad \boldsymbol{\Sigma}_{\mu\upsilon} \cdot \boldsymbol{N} + \boldsymbol{\Sigma}_\mu \cdot \boldsymbol{N}_\upsilon = 0 \\ \boldsymbol{\Sigma}_{\upsilon\mu} \cdot \boldsymbol{N} + \boldsymbol{\Sigma}_\upsilon \cdot \boldsymbol{N}_\mu = 0 \qquad \boldsymbol{\Sigma}_{\upsilon\upsilon} \cdot \boldsymbol{N} + \boldsymbol{\Sigma}_\upsilon \cdot \boldsymbol{N}_\upsilon = 0 \end{aligned} \tag{6}$$

II can be written as,

$$\begin{aligned} II &= -\boldsymbol{\Sigma}_\mu \cdot \boldsymbol{N}_\mu (\mathrm{d}\mu)^2 - 2\boldsymbol{\Sigma}_\mu \cdot \boldsymbol{N}_\upsilon \mathrm{d}\mu\mathrm{d}\upsilon - \boldsymbol{\Sigma}_\upsilon \cdot \boldsymbol{N}_\upsilon (\mathrm{d}\upsilon)^2 \\ &= \boldsymbol{\Sigma}_{\mu\mu} \cdot \boldsymbol{N} (\mathrm{d}\mu)^2 + 2\boldsymbol{\Sigma}_{\mu\upsilon} \cdot \boldsymbol{N} \mathrm{d}\mu\mathrm{d}\upsilon + \boldsymbol{\Sigma}_{\upsilon\upsilon} \cdot \boldsymbol{N} (\mathrm{d}\upsilon)^2 \end{aligned} \tag{7}$$

If the two principal directions of this curved surface which are defined as $(\boldsymbol{e}_1, \boldsymbol{e}_2)$ are coincident with coordinates directions $(\boldsymbol{t}_\mu, \boldsymbol{t}_\upsilon)$ at every point, the second fundamental form II can be expressed by two principal curvatures κ_1 and κ_2,

$$II = \kappa_1 \boldsymbol{\Sigma}_\mu \cdot \boldsymbol{\Sigma}_\mu (\mathrm{d}\mu)^2 + \kappa_2 \boldsymbol{\Sigma}_\upsilon \cdot \boldsymbol{\Sigma}_\upsilon (\mathrm{d}\upsilon)^2 \tag{8}$$

Combine Eqs. (7) and (8), the two principal curvatures κ_1 and κ_2 can be obtained,

$$\begin{aligned} \kappa_1 &= \tfrac{\boldsymbol{\Sigma}_{\mu\mu} \cdot \boldsymbol{N}}{\boldsymbol{\Sigma}_\mu \cdot \boldsymbol{\Sigma}_\mu} \\ \kappa_2 &= \tfrac{\boldsymbol{\Sigma}_{\upsilon\upsilon} \cdot \boldsymbol{N}}{\boldsymbol{\Sigma}_\upsilon \cdot \boldsymbol{\Sigma}_\upsilon} \end{aligned} \tag{9}$$

If the angle ξ is confirmed, one wire curve will be fixed, coordinates μ and υ will hold a specific relation. Let μ be the only parameter of this curve, considering the arc length s by definition is,

$$s(\mu) = \int_{\mu_0}^{\mu} \left|\frac{\mathrm{d}\boldsymbol{\Sigma}(\mu)}{\mathrm{d}\mu}\right| \mathrm{d}\mu \tag{10}$$

This yields the following expressions between arc length s and surface coordinate μ,

$$\left(\frac{\mathrm{d}s}{\mathrm{d}\mu}\right)^2 = \left(\left|\frac{\mathrm{d}\boldsymbol{\Sigma}}{\mathrm{d}\mu}\right|\right)^2 = \sqrt{\left(\frac{\mathrm{d}x}{\mathrm{d}\mu}\right)^2 + \left(\frac{\mathrm{d}y}{\mathrm{d}\mu}\right)^2 + \left(\frac{\mathrm{d}z}{\mathrm{d}\mu}\right)^2} \tag{11}$$

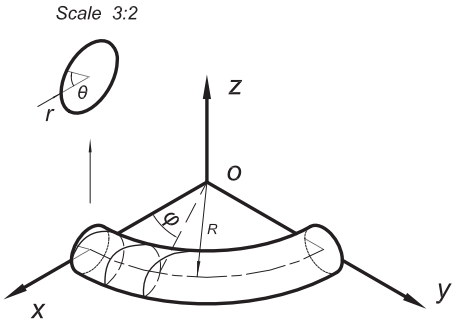

Fig. 3. Mathematical Model of a bent cylinder.

The kinematic description of moving Darboux frame (***T, N, B***) with respect to arc length s is defined as

$$\mathrm{d}\begin{bmatrix}\boldsymbol{T}\\ \boldsymbol{N}\\ \boldsymbol{B}\end{bmatrix}=\begin{bmatrix}0 & \kappa_n\mathrm{d}s & \kappa_g\mathrm{d}s\\ -\kappa_n\mathrm{d}s & 0 & -\tau_g\mathrm{d}s\\ -\kappa_g\mathrm{d}s & \tau_g\mathrm{d}s & 0\end{bmatrix}\begin{bmatrix}\boldsymbol{T}\\ \boldsymbol{N}\\ \boldsymbol{B}\end{bmatrix} \tag{12}$$

Where κ_g is geodesic curvature, κ_n is normal curvature and τ_g is geodesic torsion of the curved surface. Geodesic curvature κ_g can be derived by Liouvile proposition,

$$\kappa_g=(\kappa_g)_1\cos\xi+(\kappa_g)_2\sin\xi-\frac{\mathrm{d}\xi}{\mathrm{d}s} \tag{13}$$

Where $(\kappa_g)_1$ and $(\kappa_g)_2$ are the geodesic curvatures of the coordinate curves $\upsilon=const.$, and $\mu=const.$, respectively. Normal curvature κ_n can be obtained by the expression which is known classically as the Euler formula,

$$\kappa_n=\kappa_1\cos^2\xi+\kappa_2\sin^2\xi \tag{14}$$

Geodesic torsion τ_g can be derived by the following expression based on do Carmo's textbook [31].

$$\tau_g=(\kappa_1-\kappa_2)\sin\xi\cos\xi \tag{15}$$

All the geometrical quantities presented above are the intrinsic features of surface and will as initial data contributes to the next analysis of mechanical parts.

3. Geometrical analysis in armour wires

3.1. Calculation of basic geometrical quantities

A parameterization of a bent cylinder surface which can be seen as an abstract mathematical model for flexible pipes is set up through the following Fig. 3.

The torus (main part of the flexible pipe) parametrical expression by Cartesian coordinates in matrix form is then given by,

$$\boldsymbol{\Sigma}(\theta,\varphi)=\begin{bmatrix}x(\theta,\varphi)\\ y(\theta,\varphi)\\ z(\theta,\varphi)\end{bmatrix}=\begin{bmatrix}(R+r\cdot\cos\theta)\cos\varphi\\ (R+r\cdot\cos\theta)\sin\varphi\\ r\cdot\sin\theta\end{bmatrix} \tag{16}$$

It can be seen that the parametrical form of this surface is controlled by two parameters θ and φ. The two parameters also enable to generate the orthogonal curvilinear lines on the surface which can better simplify the differential geometry model. For convenience, the curvilinear lines are demonstrated implicitly in the paper. Then,the helical curve which is considered as the mathematical model of one single armour wire is embedded on this surface. However, due to uncertainty of the bending condition which is restricted by external force, the relationship between two parameters θ and φ which can demonstrate the curve's parameterization is now unclear. The geometrical pattern of the curve will be explicit only if the mechanical part is finished.

By substituting Eq. (16) into all equations from preliminaries part, a set of results can be presented below,

$$\boldsymbol{N}=\frac{\boldsymbol{\Sigma}_\theta\times\boldsymbol{\Sigma}_\varphi}{|\boldsymbol{\Sigma}_\theta\times\boldsymbol{\Sigma}_\varphi|}=\begin{bmatrix}-\cos\theta\cos\varphi\\ -\cos\theta\sin\varphi\\ -\sin\theta\end{bmatrix} \tag{17}$$

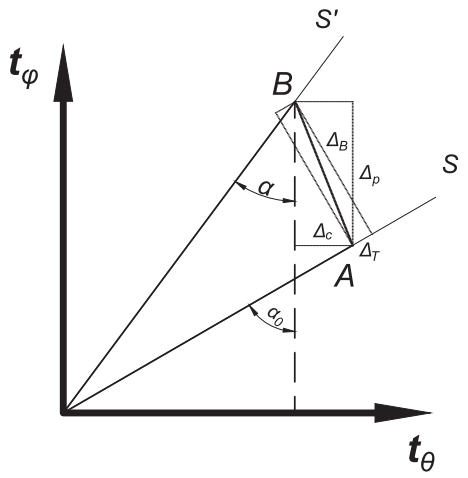

Fig. 4. geometrical interpretation for wires' slip.

$$\begin{aligned}\boldsymbol{T} &= \cos\xi\frac{\boldsymbol{\Sigma}_\theta}{|\boldsymbol{\Sigma}_\theta|} + \sin\xi\frac{\boldsymbol{\Sigma}_\varphi}{|\boldsymbol{\Sigma}_\varphi|} \\ &= \cos\xi\begin{bmatrix}-\sin\theta\cos\varphi\\ -\sin\theta\sin\varphi\\ \cos\theta\end{bmatrix} + \sin\xi\begin{bmatrix}-\sin\varphi\\ \cos\varphi\\ 0\end{bmatrix}\end{aligned} \tag{18}$$

Let $\boldsymbol{t}_\theta$ be the unit vector generated by surface derivative $\boldsymbol{\Sigma}_\theta$. Then in the above expression ξ is the angle from $\boldsymbol{t}_\theta$ to $\boldsymbol{T}$ by definition.

The relation between arc length s and coordinate θ can be derived by

$$\left(\frac{\mathrm{d}s}{\mathrm{d}\theta}\right)^2 = \left(\left|\frac{\mathrm{d}\boldsymbol{\Sigma}}{\mathrm{d}\theta}\right|\right)^2 = r^2 + (R + r\cdot\cos\theta)^2\left(\frac{\mathrm{d}\varphi}{\mathrm{d}\theta}\right)^2 \tag{19}$$

Two principal curvatures κ_1 and κ_2 are

$$\begin{aligned}\kappa_1 &= \frac{\boldsymbol{\Sigma}_{\theta\theta}\cdot\boldsymbol{N}}{\boldsymbol{\Sigma}_\theta\cdot\boldsymbol{\Sigma}_\theta} = \frac{1}{r}\\ \kappa_2 &= \frac{\boldsymbol{\Sigma}_{\varphi\varphi}\cdot\boldsymbol{N}}{\boldsymbol{\Sigma}_\varphi\cdot\boldsymbol{\Sigma}_\varphi} = \frac{\cos\theta}{R + r\cos\theta}\end{aligned} \tag{20}$$

Then κ_n, κ_g and τ_g can be obtained by using the values of κ_1 and κ_2.

$$\begin{aligned}\kappa_n &= -\frac{R}{r(R + r\cdot\cos\theta)}\sin^2\xi + \frac{1}{r}\\ \kappa_g &= -\frac{\sin\theta}{R + r\cdot\cos\theta}\sin\xi - \frac{\mathrm{d}\xi}{\mathrm{d}s}\\ \tau_g &= \frac{R}{r(R + r\cdot\cos\theta)}\cos\xi\sin\xi\end{aligned} \tag{21}$$

3.2. Interpretation for geometrical assumption

Since it is now not allowed to obtain the explicit relation between parameters θ and φ, a geometrical assumption is introduced here to illustrate the correlation. A diagrammatic sketch of the geometrical evolution by wires' slip can be demonstrated by the following Fig. 4.

In the figure, a very small moving process of one single wire is captured from curve S to S'. The movement is slight enough that the basic plane geometry relations still hold in this case. Let α be the angle between helix direction and $\boldsymbol{t}_\varphi$. Then the initial angle of α can be denoted by α_0.

A point on the curve is assumed to move from A to B. This moving trace can be decomposed into $\mathrm{d}\Delta_c$ and $\mathrm{d}\Delta_p$, which represent the unit displacement of the helix (relatively to the torus) along a parallel (θ constant), and displacement along a meridian (φ constant), $\Delta_c = r\cdot(\theta_\kappa - \theta_0)$, respectively. On the other hand, it can be also replaced by two other displacement components $\mathrm{d}\Delta_B$ and $\mathrm{d}\Delta_T$, which are unit displacements along $\boldsymbol{B}$ and $\boldsymbol{T}$ directions based on the position of initial helix.

Considering the triangle which contains the initial helical angle α_0, it is feasible to develop a trigonometric function relation using two right-angle sides of the triangle. The length of the perpendicular side can be calculated by subtracting the extra length which can be easily expressed by the unit displacement components $\mathrm{d}\Delta_p$ and $\mathrm{d}\Delta_c$. Then the following tangent relation can be established by,

$$\frac{r\cdot \mathrm{d}\theta}{R\cdot \mathrm{d}\varphi-(\mathrm{d}\Delta_p-\cot\alpha_0\cdot \mathrm{d}\Delta_c)}=\tan\alpha_0 \tag{22}$$

Note that the unit displacement components $\mathrm{d}\Delta_p$ and $\mathrm{d}\Delta_c$ are vectors pointing to specific directions. Hence, when calculating the vertical distance between two curves s and s', which is the denominator of the above equation, it is of vital importance to add the negative sign before $\mathrm{d}\Delta_c$.

Since the following conversion formula between two forms of unit displacement components ($\mathrm{d}\Delta_B$, $\mathrm{d}\Delta_T$) and ($\mathrm{d}\Delta_c$, $\mathrm{d}\Delta_p$) is satisfied,

$$\begin{bmatrix}\mathrm{d}\Delta_B\\ \mathrm{d}\Delta_T\end{bmatrix}=\begin{bmatrix}\cos\alpha_0 & -\sin\alpha_0\\ \sin\alpha_0 & \cos\alpha_0\end{bmatrix}\begin{bmatrix}\mathrm{d}\Delta_c\\ \mathrm{d}\Delta_p\end{bmatrix} \tag{23}$$

Eq. (22) can be further simplified by the following expression which brings to the relation between two parameters θ and φ,

$$\begin{aligned}\frac{\mathrm{d}\varphi}{\mathrm{d}\theta}&=\frac{r}{R\cdot\tan\alpha_0}\left[1+\frac{1}{r}\left(\tan\alpha_0\frac{\mathrm{d}\Delta_p}{\mathrm{d}\theta}-\frac{\mathrm{d}\Delta_c}{\mathrm{d}\theta}\right)\right]\\ &=\frac{r}{R\cdot\tan\alpha_0}\left(1-\frac{1}{r\cdot\cos\alpha_0}\cdot\frac{\mathrm{d}\Delta_B}{\mathrm{d}\theta}\right)\end{aligned} \tag{24}$$

It is shown in Eq. (24) that the relation between two coordinates θ and φ can be written as a form controlled by the variation of displacement component along $\boldsymbol{B}$ direction. This geometrical expression is also included in [11] and [26]. However, the distinction between helical angle and initial helical angle was not emphasized in the contents. Only original helical angle which is a constant was adopted to participate in the final implementation. Based on comprehensive discussion in geometrical part, an interpretation for this geometrical assumption is obtained. In Eq. (24), α_0 represents the initial helical angle which is always a constant while the pipe is bending. Considering the variable helical angle α which is now an unknown quantity, more geometrical research is in demand to illuminate the variation mechanism.

3.3. Further discussion of the mathematical model

Since Eq. (24) provides a connection between parametrical coordinates and lateral displacement, the key to variable wire angle α is to build up the relation between wire angle α and parametrical coordinates.

Based on Eq. (3), the tangent vector of a curve embedded on a surface can be written by variable helical angle with the following form,

$$\boldsymbol{T}=\sin\alpha\cdot\boldsymbol{e}_1+\cos\alpha\cdot\boldsymbol{e}_2 \tag{25}$$

Where, $\boldsymbol{e}_1$, $\boldsymbol{e}_2$ represent the unit vectors generated by two parameters of a specific surface.

From the definition of surface, the following must hold,

$$\frac{\mathrm{d}\boldsymbol{\Sigma}(\theta,\varphi)}{\mathrm{d}s}=\boldsymbol{T}=\boldsymbol{\Sigma}_\theta\frac{\mathrm{d}\theta}{\mathrm{d}s}+\boldsymbol{\Sigma}_\varphi\frac{\mathrm{d}\varphi}{\mathrm{d}s} \tag{26}$$

Since,

$$\begin{aligned}\boldsymbol{e}_1&=\frac{\boldsymbol{\Sigma}_\theta}{|\boldsymbol{\Sigma}_\theta|}\\ \boldsymbol{e}_2&=\frac{\boldsymbol{\Sigma}_\varphi}{|\boldsymbol{\Sigma}_\varphi|}\end{aligned} \tag{27}$$

Combining Eqs. (25), (26) and (27),

$$\begin{aligned}\frac{\mathrm{d}\theta}{\mathrm{d}s}&=\frac{\sin\alpha}{|\boldsymbol{\Sigma}_\theta|}=\frac{\sin\alpha}{r}\\ \frac{\mathrm{d}\varphi}{\mathrm{d}s}&=\frac{\cos\alpha}{|\boldsymbol{\Sigma}_\varphi|}=\frac{\cos\alpha}{R+r\cos\theta}\end{aligned} \tag{28}$$

The relation between wire angle α and parametrical coordinates is as follows,

$$\frac{\mathrm{d}\varphi}{\mathrm{d}\theta}=\frac{r}{(R+r\sin\theta)}\cot\alpha \tag{29}$$

Thus the relation between variable wire angle α and parametrical coordinates (θ, φ) is built up. Considering Eq. (24) with Eq. (29), then,

$$\frac{\mathrm{d}\Delta_B}{\mathrm{d}\theta} = A(\theta)\cdot\cot\alpha + B(\theta) \tag{30}$$

Where $A(\theta)$ and $B(\theta)$ are expressions controlled by parameter θ, which are the simplified forms of specific coefficients derived from Eqs. (24) and (29). $A(\theta)$ and $B(\theta)$ can be directly obtained by above derivation.

In order to establish a unified form in accordance with preliminaries part, the quantity ξ which represents the variable angle between $\boldsymbol{T}$ and $\boldsymbol{t}_\theta$ is chosen to replace α in the above equation. Note that, ξ is always the complement angle of α, then Eq. (30) will change into the following form,

$$\frac{\mathrm{d}\Delta_B}{\mathrm{d}\theta} = A(\theta)\cdot\tan\xi + B(\theta) \tag{31}$$

By expanding $\tan\xi$ in terms of ξ at point ξ_0 which denotes the initial angle of ξ when the pipe is unbent, a linear expression can be obtained by eliminating second and higher order terms of Taylor series. The linearized expression is given by,

$$\tan\xi = \tan\xi_0 + \frac{1}{\cos^2\xi_0}(\xi - \xi_0) \tag{32}$$

Then,

$$\frac{\mathrm{d}\Delta_B}{\mathrm{d}\theta} = A'(\theta)\cdot\xi + B'(\theta) \tag{33}$$

Where $A'(\theta)$ and $B'(\theta)$ are the improved form of coefficients $A(\theta)$ and $B(\theta)$ based on Eqs. (31) and (32).

If the angle ξ is confirmed, one wire curve can be fixed. θ and φ will hold a specific relation. Let θ be the only parameter of this curve, this yields the following expressions, which is essential for next theoretical discussion.

$$\left(\frac{\mathrm{d}s}{\mathrm{d}\theta}\right)^2 = \left(\left|\frac{\mathrm{d}\boldsymbol{\Sigma}}{\mathrm{d}\theta}\right|\right)^2 = r^2 + (R + r\cdot\cos\theta)^2\left(\frac{\mathrm{d}\varphi}{\mathrm{d}\theta}\right)^2 = \left(\frac{r}{\cos\xi}\right)^2 \tag{34}$$

So far, the geometrical system is well organized by introducing the variable helical angle of armour wires. It is a remarkable fact that Leroy and Estrier [12] had made an effort to bring lateral displacement into the theoretical system, which was also cited in [26]. The developed theory provided a novel perspective to allow a binormal movement of armour wires corresponding to the bending process. In other words, the helical angle of armour wires was changing. However, in these theoretical models none of the equations could indicate the changing process of helical angle owing to the chosen constant quantity of initial helical angle. Eq. (33) offers a connection between wires' slip and variable helical angle in this differential geometry model, which can be also used in next frictional discussion of armour wires. To solve the differential system it is possible to have access to the exact value of helical angle's variation, which will contribute to the analytical expression of resultant moment and further global bending analysis.

4. Strain analysis before and after wires' slip

In this part, a clear demonstration of strain process in armour wires is presented. In conventional theory, the expression of strain ε is the following form, which can be seen in the literature such as [5,29].

$$\varepsilon = -r\cdot\cos^2\alpha\sin\theta\cdot\kappa \tag{35}$$

However, there is an essential prerequisite to guarantee the validity of this equation. That is, slip of armour wires cannot occur when the pipe is bent. The following discussion will emphasize this distinction of strain conditions before and after slip. Two independent expressions of wires' strain will be given herein.

First of all, the perfect helix on unbent cylinder is investigated. A parameterization of an unbent cylinder surface can be established based on Fig. 3 and Eq. (16),

$$\boldsymbol{\Sigma}(\theta,\xi) = \begin{bmatrix} x(\theta,\xi_0) \\ y(\theta,\xi_0) \\ z(\theta,\xi_0) \end{bmatrix} = \begin{bmatrix} R + r\cdot\cos\theta \\ r\cdot\tan\xi_0\cdot\theta \\ r\cdot\sin\theta \end{bmatrix} \tag{36}$$

Since it is an unbent cylinder, the parameter ξ_0 is determined in the above equation instead of φ. As is mentioned in previous part, ξ_0 is the angle between $\boldsymbol{T}$ and $\boldsymbol{t}_\theta$. The subscript 0 indicates that the parameter is a constant. The surface will therefore degenerate into a curve, which is controlled by only one parameter θ.

Then the arc length which can be represented by s_1 is given based on Eqs. (10) and (36),

$$s_1 = \int_{\theta_0}^{\theta}\left|\frac{\mathrm{d}\boldsymbol{\Sigma}(\theta)}{\mathrm{d}\theta}\right|\mathrm{d}\theta = \int_0^{\theta}\sqrt{\frac{r^2}{\cos^2\xi_0}}\mathrm{d}\theta \tag{37}$$

According to different scenarios before and after armour wires' slip, the strain analysis in bending situation is therefore separated into the following two parts.

4.1. Strain analysis before armour wires' slip

If no slip occurs during the bending process, the helical wires will be fixed on the torus, the geometrical relation between θ and φ remains in the unbent situation, which is still compatible with the rule in plane triangle,

$$\frac{\mathrm{d}\varphi}{\mathrm{d}\theta} = \frac{r}{R}\tan\xi_0 \tag{38}$$

Then, the arc length s_2 can be obtained by Eqs. (10) and (16),

$$s_2 = \int_0^\theta \sqrt{r^2 + (R + r\cdot\cos\theta)^2\left(\frac{\mathrm{d}\varphi}{\mathrm{d}\theta}\right)^2}\,\mathrm{d}\theta = \int_0^\theta \sqrt{r^2 + (R + r\cdot\cos\theta)^2\cdot\frac{r^2\tan^2\xi_0}{R^2}}\,\mathrm{d}\theta \tag{39}$$

Finally, the strain of one single armour wire before wires' slip can be calculated by,

$$\begin{aligned}\varepsilon_1 &= \frac{\mathrm{d}s_2}{\mathrm{d}s_1} - 1 = \sqrt{\cos^2\xi_0 + (1 + r\cdot\kappa\cos\theta)^2\cdot\sin^2\xi_0} - 1\\ &= \sqrt{1 + 2r\cdot\sin^2\xi_0\cos\theta\cdot\kappa + r^2\sin^2\xi_0\cos^2\theta\cdot\kappa^2} - 1\end{aligned} \tag{40}$$

Using Taylor's formula, this expression can be simplified by expanding it in terms of κ at point 0,

$$\varepsilon_1 \approx r\cdot\sin^2\xi_0\cos\theta\cdot\kappa \tag{41}$$

By unifying the mathematical descriptions such as the definition of helical angle of armour wires in a specific parametrical model, the obtained expression of strain is identical with Eq. (35). Moreover, based on detailed derivation, in order to satisfy the expression, two main prerequisites are revealed. Firstly, this strain expression can be used only in non-slippage situation due to Eq. (38). Secondly, this strain expression cannot hold in large bending situation due to the limitation of Taylor's formula.

4.2. Strain analysis after armour wires' slip

Based on above discussion and limitations, it is essential to move forward to the study of strain after armour wires' slip, which will be more compatible with the case in large bending situation.

In slippage region, Eq. (29) which denotes the geometrical relation between θ and φ is applied to participate in the implementation rather than Eq. (38), since the helical wires will no longer be fixed on the torus.

Arc length s_2 can still be calculated with the same process as that in Eq. (39). Then the strain of one single armour wire after wires' slip can be given by,

$$\varepsilon_2 = \frac{\sqrt{\frac{r^2}{\cos^2\xi}}}{\sqrt{\frac{r^2}{\cos^2\xi_0}}} - 1 = \sqrt{\frac{\cos^2\xi_0}{\cos^2\xi}} - 1 \tag{42}$$

By expanding the above equation in terms of ξ at point ξ_0, the linearized strain expression after wires' slip is obtained,

$$\varepsilon_2 \approx \tan\xi_0(\xi - \xi_0) \tag{43}$$

To sum up, based on detailed discussion and induction in strain analysis, the conventional theory of armour wires' strain is modified. Eq. (41) which represents the strain of armour wires can be only applied in wires' non-slippage region. After wires' slip occurs, Eq. (41) will be replaced by Eq. (43) to calculate the accurate strain of armour wires.

Note that, the critical curvature which determines the exact time of wires' slip is of vital importance since the variation of helical angle occurs after this curvature in the bending process. However, it is only a criterion which does not affect the mechanism analysis of variable helical angle of armour wires. Hence, the discussion of critical curvature will be put in later part.

5. Mechanical analysis

In mechanical part, the analysis is based on existing theory of curved beam which can be seen in the literature such as [12,17,26]. Three parts including equilibrium equations, constitutive relations and friction study will be introduced as follows.

5.1. Equilibrium equations

Based on curved beam theory on vectorial form which is widely used by many authors such as Erichsen and Truesdell [32], Reissner [33] and Love [34], the componentwise equations of equilibrium along the local frame (***T***, ***N***, ***B***) can be obtained by,

$$\frac{\mathrm{d}F_T}{\mathrm{d}s} - \kappa_n F_N - \kappa_g F_B + p_T = 0 \tag{44}$$

$$\frac{dF_N}{ds} + \kappa_n F_T + \tau_g F_B + p_N = 0 \tag{45}$$

$$\frac{dF_B}{ds} + \kappa_g F_T - \tau_g F_N + p_B = 0 \tag{46}$$

$$\frac{dM_T}{ds} - \kappa_n M_N - \kappa_g M_B + m_T = 0 \tag{47}$$

$$\frac{dM_N}{ds} + \kappa_n M_T + \tau_g M_B - F_B + m_N = 0 \tag{48}$$

$$\frac{dM_B}{ds} + \kappa_g M_T - \tau_g M_N + F_N + m_B = 0 \tag{49}$$

Where, κ_g, κ_n and τ_g can be derived by Eq. (21). F_T, F_N, F_B and M_T, M_N, M_B represent the component sectional forces and moments along directions of ***T, N, B*** respectively. Similarly, p_T, p_N, p_B and m_T, m_N, m_B respectively represent the component distributed forces and moments along the same local directions.

5.2. Constitutive relations

The constitutive relations in helical wires are listed below to combine forces and deformations,

$$F_T = EA\varepsilon \tag{50}$$

$$M_B = EI_B \Delta\kappa_n \tag{51}$$

$$M_N = -EI_N \Delta\kappa_g \tag{52}$$

$$M_T = -GI_\rho \Delta\tau_g \tag{53}$$

Where E and G respectively represent elastic and shear moduli. A is the cross sectional area of the wire. I_B, I_N, I_ρ are the wire second moments of area. These quantities are known as constants when applying a specific case.

$\Delta\kappa_g$, $\Delta\kappa_n$ and $\Delta\tau_g$ are the changes of curvatures corresponding to the bending process. When the pipe is unbent, the initial curvature components which is denoted by κ_n^0, κ_g^0 and τ_g^0 can be calculated by letting $\frac{1}{R} = 0$ in Eq. (21),

$$\begin{aligned} \kappa_n^0 &= \frac{\cos^2 \xi_0}{r} \\ \kappa_g^0 &= 0 \\ \tau_g^0 &= \frac{\cos \xi_0 \sin \xi_0}{r} \end{aligned} \tag{54}$$

Then $\Delta\kappa_g$, $\Delta\kappa_n$ and $\Delta\tau_g$ can be given by,

$$\Delta\kappa_n = \kappa_n - \kappa_n^0 = -\frac{R}{r(R + r\cdot\cos\theta)} \sin^2 \xi + \frac{\sin^2 \xi_0}{r} \tag{55}$$

$$\Delta\kappa_g = \kappa_g - \kappa_g^0 = -\frac{\sin\theta}{R + r\cdot\cos\theta} \sin\xi - \frac{d\xi}{ds} \tag{56}$$

$$\Delta\tau_g = \tau_g - \tau_g^0 = \frac{R}{r(R + r\cdot\cos\theta)} \cos\xi \sin\xi - \frac{\cos\xi_0 \sin\xi_0}{r} \tag{57}$$

It is noted that in Eq. (50) the tangential force F_T is only suitable for pure bending. If initial tensile force is applied, Eq. (50) can be modifed by,

$$F_T = EA\varepsilon + F_t^{ini} \tag{58}$$

Since the expression of strain is modified in the above part, it is apparently shown that the chosen of strain's expression will show influence on the final result of tangential force F_T. In other words, the mechanical analysis which contains the effect of variable helical angle of armour wires will exhibit two independent scenarios before and after armour wires' slip.

5.3. Analysis of friction

In equilibrium equations, frictional force cannot be applied in direct form. Considering one layer of armour wires, Coulomb friction is chosen to set up the frictional model of armour wires. The following scalar components $q_{f,T}$ and $q_{f,B}$

(per unit length of a helix) are the orthogonal projections of friction force onto the two unit vectors in the directions of $\boldsymbol{T}$ and $\boldsymbol{B}$ respectively, which also represent p_T and p_B in Eqs. (44) and (46).

$$q_{f,T} = p_T = \frac{\dot{\Delta}_T}{\sqrt{\dot{\Delta}_T^2 + \dot{\Delta}_B^2}} \cdot f \cdot p_N \tag{59}$$

$$q_{f,B} = p_B = \frac{\dot{\Delta}_B}{\sqrt{\dot{\Delta}_T^2 + \dot{\Delta}_B^2}} \cdot f \cdot p_N \tag{60}$$

Where, f is the friction coefficient between interfaces, p_N is the contact pressure (per unit length of a helix) which is also the normal force in Eq. (45). $\dot{\Delta}_T$ and $\dot{\Delta}_B$ can be written as

$$\dot{\Delta}_T = \frac{\partial \Delta_T}{\partial \kappa} \tag{61}$$

$$\dot{\Delta}_B = \frac{\partial \Delta_B}{\partial \kappa} \tag{62}$$

The derivative form denotes sliding velocity of armour wires with respect to bending curvature κ. This approach of friction on armour wires is followed by [12,26].

6. Solution

Based on above geometrical and mechanical analyses, a theoretical system of this engineering model is revealed. Considering the different scenarios before and after wires' slip, the solution is also divided into the following two parts.

6.1. Before armour wires' slip

In non-slippage situation, helical angle of armour wires in flexible pipes is a constant. The unknown quantities in this scenario are all kinds of component forces and moments which can be calculated by equilibrium equations. Although these unknown quantities are not emphasis in the bending problem of flexible pipes, the critical curvature which determines the time of wires' slip can be calculated in this scenario.

According to the equilibrium relation of armour wires in tensile armour layers, the wires remain relative static unless the following equation is not satisfied,

$$\frac{\mathrm{d}F_T}{\mathrm{d}s} < q_f \tag{63}$$

Where, F_T denotes the tangential force of one single armour wire. q_f represents the frictional force(per unit length of a helix).

When pure bending is applied in the case, the left side of the above equation can be given by,

$$\frac{\mathrm{d}F_T}{\mathrm{d}s} = \frac{\mathrm{d}(EA\varepsilon_1)}{\mathrm{d}\theta} \cdot \frac{\mathrm{d}\theta}{\mathrm{d}s} = EA \sin^2 \xi_0 \cos \xi_0 \cos \theta \cdot \kappa \tag{64}$$

This equation describes the variation of tangential force with respect to arc length. It can be seen that the tangential force of armour wires is controlled by two variable parameters, which are the parametrical coordinate θ and the global curvature κ. When a specific curvature κ is given, the maximum of tangential force is obtained by letting $\theta = 0$ in the above equation. Then the critical curvature which is represented by κ_{cr} can be calculated,

$$\kappa_{cr} = \frac{q_f}{EA \sin^2 \xi_0 \cos \xi_0} = \frac{f p_N}{EA \sin^2 \xi_0 \cos \xi_0} \tag{65}$$

Generally, by knowing the axial tensile force of flexible pipes, the tangential component force on each single armour wire can be obtained. Then according to equilibrium equations in unbent condition, the relation between tangential force F_T and contact pressure p_N is given herein. By substituting the value of tangential force F_T into this relation, the final critical curvature κ_{cr} can be calculated with the obtained value of contact pressure p_N.

6.2. After armour wires' slip

When armour wires begin to slip along the torus, the study keystone is to calculate the variable helical angle of armour wires in flexible pipes. In this bent scenario, all available equations corresponding to the unknown quantity ξ are included in above discussion, which are Eqs. (55) to (57), Eqs. (43), (33) and (32). They represent the variations of component curvatures, the strain of armour wires in slippage region, the relation between arc length s and parametrical coordinate θ and the

relation between lateral displacement Δ_B and variable helical angle ξ, respectively. The other related equations include the equilibrium Eqs. (44)–(49), the constitutive relations (50)–(53) and the frictional expressions (59) and (60).

Note that, the current partial differential system is complex to find exact solution. Based on previous discussion in [26], this theoretical system exhibits a linear tendency with respect to bending curvature κ within one cycle of the bending process. Hence two approximate equations are given here to simplify the model, $\dot{\Delta}_T \approx \frac{\Delta_T}{\kappa}$, $\dot{\Delta}_B \approx \frac{\Delta_B}{\kappa}$, which transform the whole system into an ordinary differential system with 18 equations.

Meanwhile, the unknown quantities are component sectional forces F_T, F_N, F_B and moments M_T, M_N, M_B, component distributed loads p_T, p_N, p_B and moments m_T, m_N, m_B, component curvatures κ_g, κ_n and τ_g, component displacements Δ_B and Δ_T, strain ε, arc length s and the variable helical angle ξ.

In conventional methods, m_N and m_B are simplified to zeros on account of their limit contribution to the system. Meanwhile, m_T can be calculated individually by Eq. (47). Formally, it is preferable to follow this approach since the number of unknown quantities can reduce to 18. Then the differential system of equations will be balanced which can be solved by searching for numerical algorithms. The boundary conditions can be assumed by setting wire slip Δ_B and Δ_T to null corresponding to the two end fittings of the flexible pipes.

7. Case study

In order to validate the established theoretical model, several published results related to local behavior of armour wires in flexible pipes are chosen here to make comparison with the proposed method. Since variable helical angle of armour wires in flexible pipes is a preliminary investigation in slip model, the emphasis of this work lies in the first half cycle of the bending process which focuses on the monotonic response. The hysteretic response can be further studied by considering the solution of the original partial differential system. Besides, one of the 2 armour layers are assumed to implement the study, which can better simulate the local behavior of armour wires by theoretical method.

7.1. Case study i: frictionless study

Stresses and slips in local armour layers of bent flexible pipes were studied in [12]. The strain of armour wires was represented as a function of tangential displacement Δ_T, which differs from other conventional theoretical descriptions,

$$\varepsilon = \frac{\sin\alpha_0}{r} \cdot \frac{\mathrm{d}\Delta_T}{\mathrm{d}\theta} + \frac{r}{R} \cdot \cos^2\alpha_0 \cdot \cos\theta \tag{66}$$

A verification of this expression can be made by comparing with Eq. (41). Considering an unbent situation of a flexible pipe, Δ_T will be null since no slip occurs in armour wires. Eq. (66) can be simplified by,

$$\varepsilon = \frac{r}{R} \cdot \cos^2\alpha_0 \cos\theta = r \cdot \sin^2\xi_0 \cos\theta \cdot \kappa \tag{67}$$

Hence, in unbent situation of flexible pipes, the expression exhibits a same form with Eq. (41).

Considering the slippage region of armour wires, combining Eq. (66) and Eq. (43), then a relation between tangential displacement Δ_T and variable helical angle of armour wires can be given by,

$$\frac{\mathrm{d}\Delta_T}{\mathrm{d}\theta} = C(\theta) \cdot \xi + D(\theta) \tag{68}$$

$C(\theta)$ and $D(\theta)$ can be directly obtained by Eq. (66) and Eq. (43). The two coefficients are introduced here also to simplify the equations. This expression is obtained by using the existing equation in [12], which can be a reasonable comparison material to testify the accuracy of the proposed theoretical model of variable helical angle of armour wires. Δ_B and Δ_T can be calculated by solving the differential system using numerical methods, which lead to the final result of variable helical angle either by Eq. (33) or the derived Eq. (68) by published reference.

As is shown in [12], the flexible pipe was subjected to a bending process from $\kappa = 0$ to $\kappa = 0.1\ \mathrm{m}^{-1}$. Considering the outer tensile armour layer, the following input data was used:

$$E = 2 \cdot 10^{11}\mathrm{Pa}, \quad A = b \cdot h = 36\mathrm{mm}^2$$
$$\alpha_0 = 35^\circ \rightarrow \xi_0 = 55^\circ, \quad r = 83.8\mathrm{mm}$$

For convenience, the differential system solved by using of a commercially available solver known as NDSolve in the Mathematica programming environment. It is superior to choose this method since the solver is fairly stable and efficient and provides easy access to the final results.

Here, let

$$\bar{\xi} = \xi - \xi_0 \tag{69}$$

Where $\bar{\xi}$ denotes the variation of helical angle, which can exhibit a final result with a zero oscillation center and it is more convenient to reveal the basic features of the variable helical angle model.

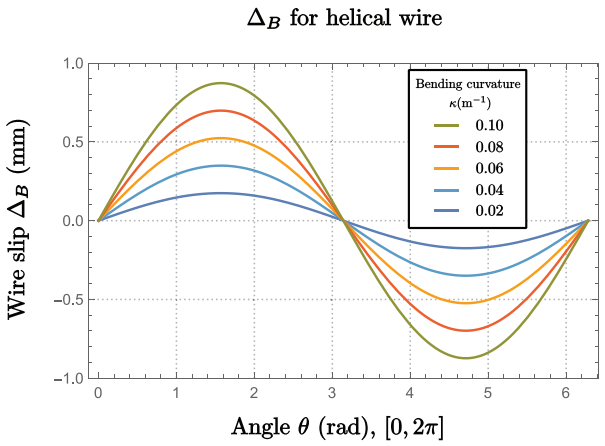

Fig. 5. Change of wire slip Δ_B in frictionless situation.

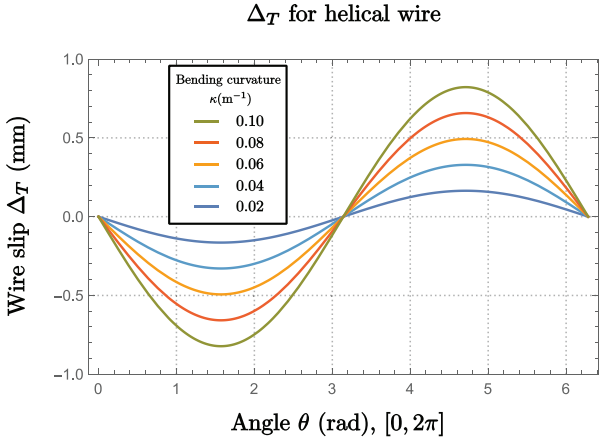

Fig. 6. Change of wire slip Δ_T in frictionless situation.

In order to validate the proposed theoretical model preliminarily, a frictionless case study is made first to investigate the feasibility of this approach. In frictionless situation, helical wires will slip from beginning of the bending process. p_T and p_N will be neglected. The differential system is conveniently solved by numerical solution in NDSolve programming environment.

Fig. 5 shows the result of lateral displacement Δ_B along parametrical coordinate θ under specific bending conditions. In the meantime, Fig. 6 shows the similar result of tangential displacement Δ_T with respect to parametrical coordinate θ. The two figures exhibit a similar sinusoidal shape. The data calculated by the system are in accordance with those in [12,26].

Fig. 7 exhibits the variable helical angles of armour wires derived both by the proposed and corresponding [12] methods, see the representations of Eqs. (33) and (68). Compared to an implementation through the lateral displacement Δ_B, it shows the similar results which derived by equations provided in [12]. From the figure it can be seen that, the values of helical angle derived by two ways are basically coincident. Therefore, it is shown that the proposed theoretical method is reliable to predict the local behavior of armour wires in flexible pipes. The mathematical solution algorithm for calculating the variable helical angle is also the main contribution of this work.

However, in this frictionless case study, the change of helical angle is very small. The oscillation curves demonstrate an amplitude of only 0.5 degrees. By scrutinizing the theoretical model with different input data, it is seen that the size of flexible pipe will show significant influence on the final result of variable helical angle. Leroy and Estrier [12] provided a small pipe with a diameter of 156.6 mm in helical layers (approximately a 6-inch pipe). The scale of this pipe makes it impossible to observe a remarkable oscillation tendency of helical angle. A case study with a larger size of flexible pipe which will be introduced in the next part is in demand.

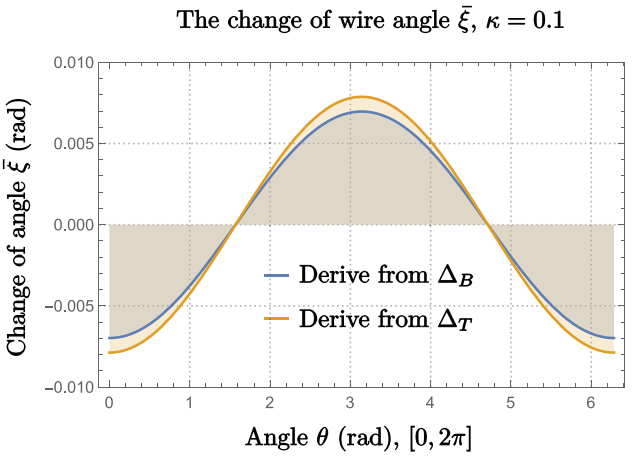

Fig. 7. Change of wire angle $\bar{\xi}$ by Δ_B and Δ_T in frictionless situation.

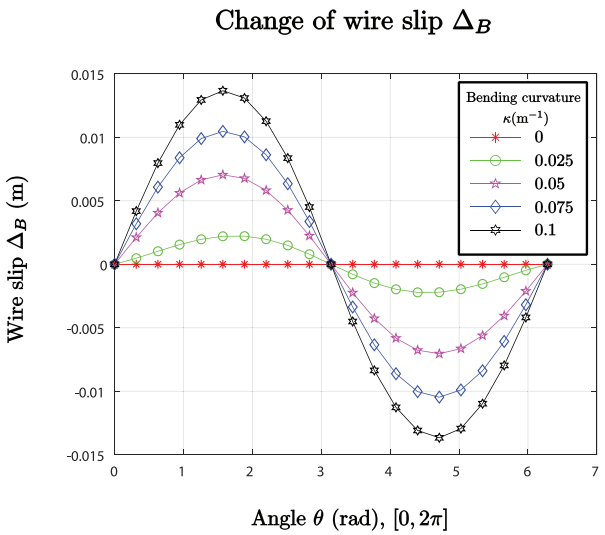

Fig. 8. Change of wire slip Δ_B in frictional situation.

7.2. Case study ii: inclusion of friction in large flexible pipe

Østergaard et al. [18] provided a larger size pipe with the following input data,

$$E = 2.1 \cdot 10^{11}\text{Pa}, \quad A = b \cdot h = 12.5 \times 5 = 62.5\text{mm}^2$$
$$\alpha_0 = 30^\circ \rightarrow \xi_0 = 60^\circ, \quad r = 276.2\text{mm}$$
$$f = 0.1, \quad F_T^{ini} = 6300\text{N}$$

In this case the frictional effect is taken into consideration. Similarly, results for lateral and tangential slips and variation in the helical angle as a function of the circumfenrential coordinate can be obtained as seen in Figs. 8–10.

It is shown that the wire slips Δ_B and Δ_T exhibit larger scales compared to *case study i* since a larger pipe is applied, although frictional effect is included. The data calculated by the theoretical system are also in accordance with those in [18]. Meanwhile, the change of helical angle is near 5° corresponding to the maximum bending curvature ($\kappa = 0.1\text{m}^{-1}$).

From [29], an analytical expression for the resultant moment of one single bent armour wire can be given by

$$M = \frac{1}{2}EAr^2 \cdot \sin^3\xi \cdot \kappa + \frac{1}{2}\left(GI_\rho \cos^2\xi + EI_N + EI_B \sin^2\xi\right)\kappa \tag{70}$$

It can be seen that the helical angle ξ is the only variable quantity in the formula. Accordingly, the slip process is therefore divided into non-slippage region and slippage region due to static friction effect between layers at the beginning of bending. Meanwhile, considering the unbent condition, p_N can be calculated by F_T^{ini} using Eq. (45). Then the critical

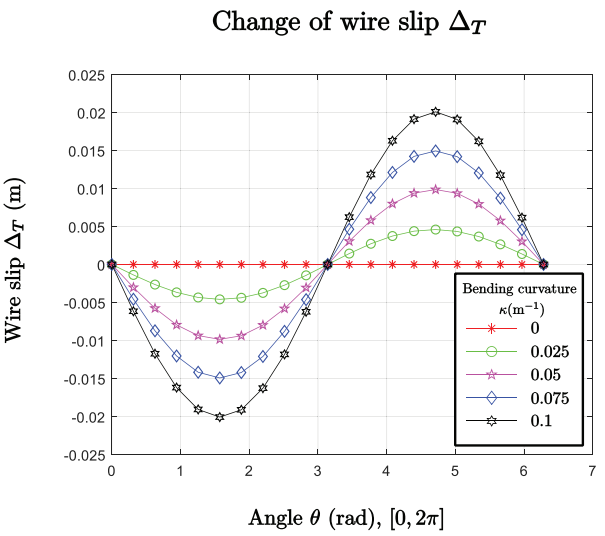

Fig. 9. Change of wire slip Δ_T in frictional situation.

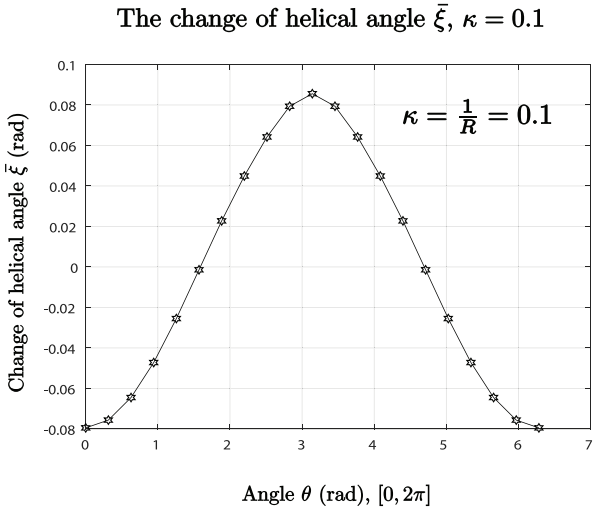

Fig. 10. Change of wire angle $\bar{\xi}$ in frictional situation.

curvature can be obtained by,

$$\kappa_{cr} = \frac{f p_N}{EA \sin^2 \xi_0 \cos \xi_0} = 0.003 \text{m}^{-1} \tag{71}$$

By using the result of helical angle's variation corresponding to the change of bending curvature, a nonlinear bending moment-curvature relation can be established. Fig. 11 describes the change of resultant moment of one single armour wire with respect to bending curvature. Due to Both scenarios of non-slippage and slippage regions are considered in this case. From the figure it can be clearly observed that the curve's slope is decreasing in the slippage region. Meanwhile, the dashed line in the figure represents the M - κ relation with no effect of the helical angle change. The corresponding curve can apparently simulate the hysteretic bending moment-curvature relation which is frequently observed in practical applications of flexible pipes.

Note that, in recent research, the hysteretic response can be also simulated by dividing the bending process into three scenarios, nonslip, progressive slip and full slip regions. Different expressions are applied to change the bending stiffness such as Witz and other authers [5,29] because of the friction and energy effects. They assumed that the armour wires could only move in geodesic direction, i.e., the constant helical angle hypothesis. Differ from the proposed method, the stiffness decreased very straight since the main "EI" was omitted when the wires began to slip. The presented method provides another perspective of global bending process which is the variable helical angle hypothesis. It can lead to a better simulation of the bending response compared to previous analytical results.

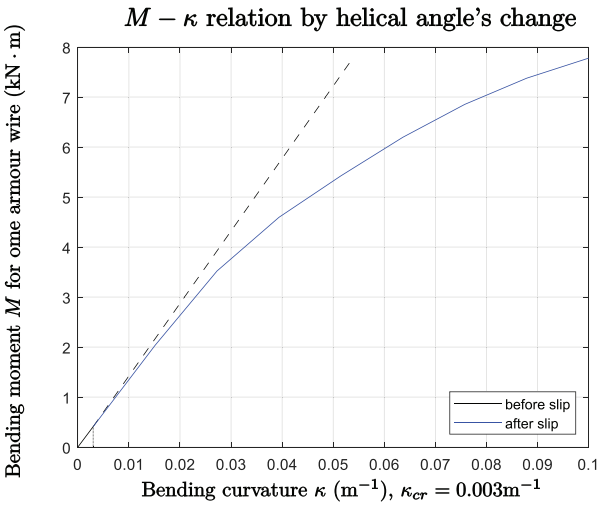

Fig. 11. $M-\kappa$ relation by helical angle's change.

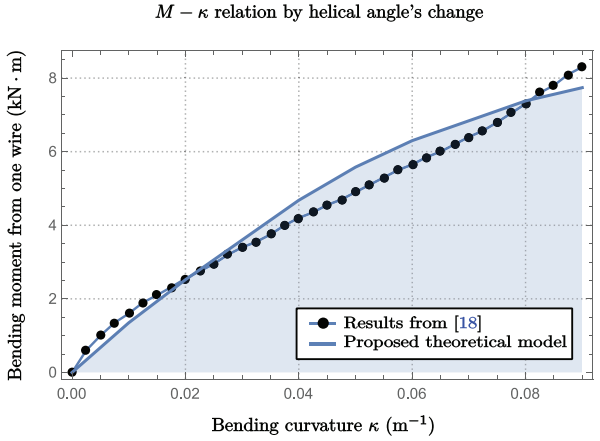

Fig. 12. resultant moment comparison of one single armour wire.

Although in [17], Østergaard at al. did not make quantitative analysis of global bending problem in flexible pipes, a numerical bending simulation research of the relation between resultant moment and curvature in one single armour wire is presented in subsequent paper [18]. In order to validate the theoretical model, a controlled verification is presented here. Without jeopardy to the comparison, it should be noted that in [18] the flexible pipe is under compression. Based on the numerical model result for the angle variation, and combining it with the analytical expression Eq. (70), the bending moment versus curvature curve for one single armour wire is plotted in Fig. 12 for the first half bending cycle together with the results from [18]. It can be seen that the results are within a certain range of error. If the variable helical angle model is not introduced here, the numerical result would be a straight line with constant slope. This will lead to a distinct divergence between the two compared results. Because of the variable helical angle, the hysteretic phenomenon of the relation between resultant moment of one single armour wire and bending curvature is occurred to confine the compared error within a specific range, especially the amplitude data.

7.3. Case study iii: experimental comparison

In order to move forward to analyze the global bending problem of flexible pipes, a comparison study with an experimental test provided in Ref. [35] is emphasized. Generally, it is not easy to observe the change of local armour wires since helical layers are internal. The comparison is based on the resultant moment of a whole flexible pipe. Moreover, in Ref. [35] the friction along longitudinal direction, i.e., one dimensional friction, is focused on in the work. That meant the work only allowed geodesic slip of helical wires. Since the FE result proposed in this literature matched the experiment test well, this could also be a comparison with the constant helical angle hypothesis. The input data was given detailedly in the literature, see Table 1.

Table 1
Input data in Ref.[35].

Parameter	Value	Unit
Barrier (Core) mean radius	58.3	mm
Pressure spiral mean radius	64.05	mm
Anti-wear tape 1 mean radius	68.2	mm
Anti-wear tape 2 mean radius	72.2	mm
Inner tensile armour mean radius	70.3	mm
outer tensile armour mean radius	74.3	mm
Tape (Nylon)	75.4	mm
Plastic layers' Young's modulus	1100	MPa
Outer sheath mean radius	78.55	mm
Pressure spiral area	35	mm^2
Steel wire's Young's modulus	210	GPa
Inner/outer tensile armour area	10	mm^2
Inner/outer tensile armour layer angle	-38/38	deg
Number of inner tensile armour	61	
Number of inner tensile armour	65	

The rest known information is as follows,

$$A = b \cdot h = 5 \times 2 = 10\text{mm}^2$$
$$\kappa : 0 \rightarrow \tfrac{1}{9} \approx 0.11\text{m}^{-1}$$
$$f = 0.26, \quad P_N^{int} = 200\text{bar} = 20\text{MPa}$$

Then, the critical curvature can be obtained by,

$$\kappa_{cr} = \frac{\mu q_N}{EA\sin^2\xi_0\cos\xi_0} = \frac{\mu P_N^{int}}{Et\sin^2\xi_0\cos\xi_0} = 0.0077\text{m}^{-1}$$

Where, t is thickness of the armour wire.

Note that, this experimental test also provided a pipe sample with small size. However, it is still feasible to observe a relatively obvious hysteretic phenomenon in $M-\kappa$ relation if the contributions of all helical wires are accumulated.

To calculate the overall resultant bending moment, contributions of every layer in the flexible pipes are therefore taken into account. The fundamental equation of a bending beam is provided as follows,

$$M = EI \cdot \kappa \tag{72}$$

The equation of a torus object's second moment of area is,

$$I_{torus} = \frac{\pi D^4}{64}\left[1 - \left(\frac{d}{D}\right)^4\right] \tag{73}$$

Where, d and D represent the internal and external radii of the torus.

Moreover, the equation of rectangle Object's second moment of area, especially for the two tensile armour layers and carcass layer are,

$$I_{rectangle} = \frac{bh^3}{12} \tag{74}$$

Where, b and h represent the length and thick of the rectangle.

For multiple layers, a simple accumulative method is chosen to obtain the global resultant moment,

$$M_{resultant} = (E_1I_1 + E_2I_2 + \cdots E_nI_n) \cdot \kappa \tag{75}$$

It is noted that in conventional solution, the calculation of one armour layer's resultant bending moment is decided by adding the same contribution of every single armour wire. Since in Ref. [35] the number of tensile armours are given in detail, it is reasonable to follow this assumption to make a controlled verification.

Using the data above, the change of helical angle can be obtained. To capture the global bending moment phenomenon, every layer in the flexible pipe is considered with the provided information in Table 1. In this case, by capturing enough points information in the comparative paper with Test No.5 Measurements, the final comparison of the global bending moment is presented in the following figure.

The compared results shown in Fig. 13 also validate the proposed theoretical model of variable helical angle of armour wires in flexible pipes. Due to limitation of the variable helical angle method, the curve's change of the proposed theoretical result is smoother than the experimental result in Ref. [35]. In the presented solution, only one equation (Eq. 70) is used to simulate the bending moment. However, the divergency of amplitude data is within a small range. The changing tendencies of both curves are similar to simulate the nonlinearities of global bending problem in flexible pipes. Furthermore, because

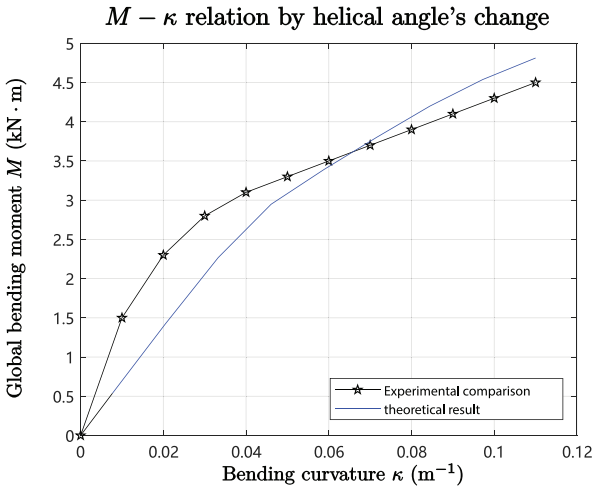

Fig. 13. $M-\kappa$ relation in resultant situation.

of the geodesic slip hypothesis, the results in Ref. [35] presented a higher stiffness tendency which is more similar to the experimental results.

In practical engineering applications, by means of the introduction of variable helical angle, a better interpretation for the bending behavior of flexible pipes is proposed. For instance, in marine environment, when cyclic bending behavior is occurred in flexible pipes, the final hysteretic phenomenon would not be well observed if all layers of flexible pipes are fixed without loxodromic slippage, since the material of armour layers is considered to be linear elastic. On the contrary, based on the proposed model which considered the influence of variable helical angle of tensile armour wires in flexible pipes, the relative slippage of armour layers and the factor of friction are also included, a comparatively more convincing perspective of local armour layers' behavior in flexible pipes is provided.

7.4. Parametric analysis

In the paper, the another cardinal goal to analyze the variable helical angle of armour wires in flexible pipes is to exhibit some new conclusions about the change of variable helical angle by controlling the values of other parameters such as initial tensile force or friction coefficient. Since the impact of variable helical angle has not been observed as a fundamental research target in previous literature, some novel rules about the behavior of armour wires may be observed.

7.5. Parametric influence on variable helical angle

In this section, four quantities are chosen as the controlled parameters to observe the variation of helical angle along the coordinate θ. These quantities are initial conditions which need to be given from the beginning of the calculation process. Therefore, changing these initial conditions will bring significant influence on the final results of helical angle while bending the pipe.

For convenience, the input data is provided by *Case Study ii*, so as to make a clear quantitative analysis around these chosen parameters.

By collecting numerical results in every calculation process while changing the chosen quantities, Figs. 14–17 are obtained to analyze the parametric influence on variable helical angle by three scenarios corresponding to the given quantity.

The first controlled parameter is initial helical angle. In a given flexible pipe, armour wires are forced to wind along a specific spiral angle. In a perfect straight pipe, the original helical angle is a constant. Since too small helical angle will bring some unstable phenomenon in the numerical solution, three appropriate values (α_0/ξ_0 - 30/60, 35/55, 40/50) presented in the figure are chosen. It can be seen in Fig. 14, α_0/ξ_0 - 30/60 is the original data used in *Case Study ii*. When increasing the value of initial helical angle, the changing of helical angle with respect to bending curvature is reduced. Considering the geometrical relation provided in Fig. 4, this result shows a reasonable phenomenon. That is, if the pipe is winded by helical wires in a tighter condition, it is harder to bend the pipe, as well as to change the helical angle. The observed phenomenon is also in accordance with other simplified equations that assume geodesic or loxodromic slip of armour wires.

The second controlled parameter is initial tensile force. This parameter is given initially to provide contact pressure between layers in flexible pipes. In Fig. 15, when distinctly increasing the value of F_t, the variable helical angle corresponding to coordinate θ does not change substantially. However, by local magnification around the peak area in Fig. 15, a decreasing tendency can be found. It is shown that, the increasing of initial tensile force can also reduce the change of helical angle with respect to bending curvature due to intensifying the contact pressure between layers in flexible pipes.

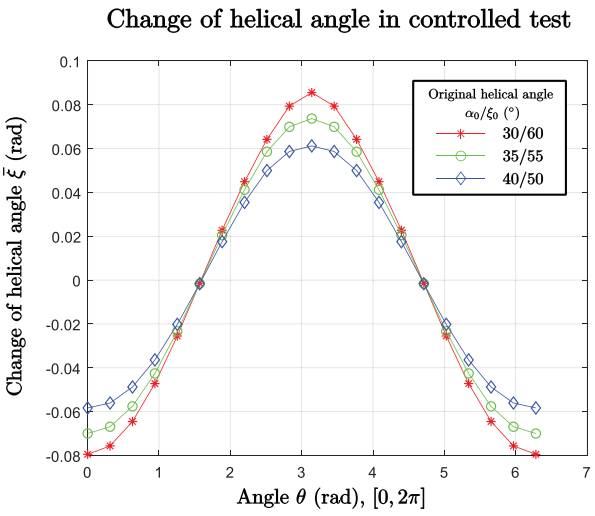

Fig. 14. Change of helical angle by controlling α_0/ξ_0.

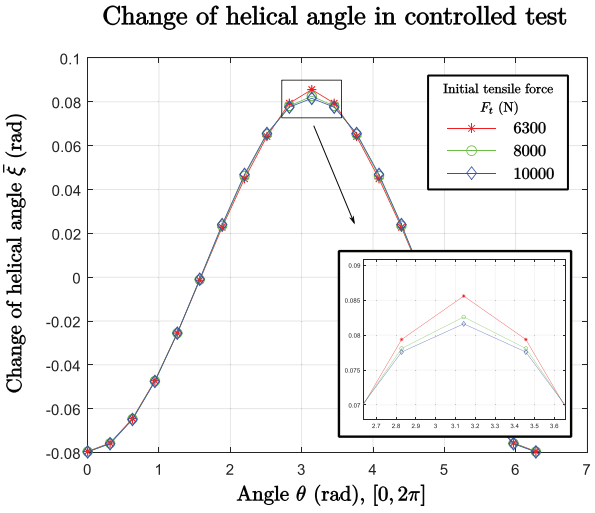

Fig. 15. Change of helical angle by controlling F_t.

The third controlled parameter is friction coefficient. If the parameter increases, the friction force between helical layer and adjacent layers will also increase. This will cause a decreasing tendency of the variable helical angle. The result shown in Fig. 16 is similar to that in Fig. 15. It shows that friction coefficient and initial tensile force have similar effects on changing the condition of helical wires. Furthermore, unlike the results in Fig. 14, it can be clearly seen in Figs. 15 and 16, these two parameters can only change the value of helical angle at the middle area corresponding to coordinate θ.

The fourth controlled parameter is bending curvature. The result of this controlled test is apparently predictable in Fig. 17. Since the increasing of bending curvature can obviously enlarge the change of armour wires, this will lead to the increasing of helical angle's change.

7.6. Parametric influence on global bending moment

After the parametric analysis on variable helical angle, it is essential to move forward to observe the results of the above controlled parameters on the global bending problem. Considering the obtained numerical results of variable helical angle, the final controlled M - κ relation in three scenarios can be given by substituting into Eq. (70). Nevertheless, in this section the bending curvature κ will become the parameter of the abscissa, choosing bending curvature as a controlled quantity to analyze is not appropriate. Hence, only original helical angle, initial tensile force and friction coefficient are determined to participate in this parametric analysis on global bending moment. Moreover, in all these studies, the impact of not considering the helical angle variation is not presented. In the representation, only Eq. 70 is considered to simulate the bending moment. The progressive slip of the wires are accounted based on summation of the contributions in Eq. 70.

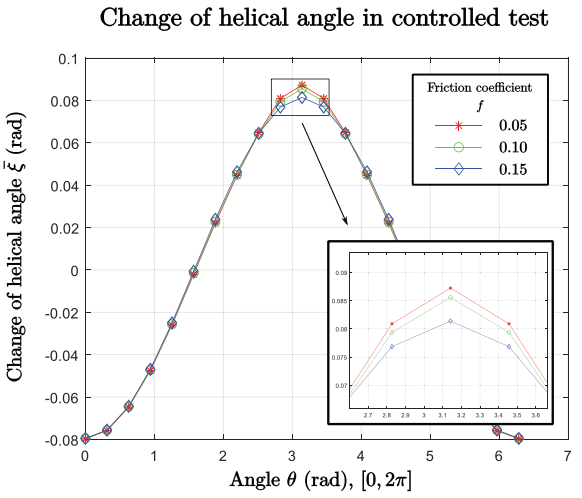

Fig. 16. Change of helical angle by controlling f.

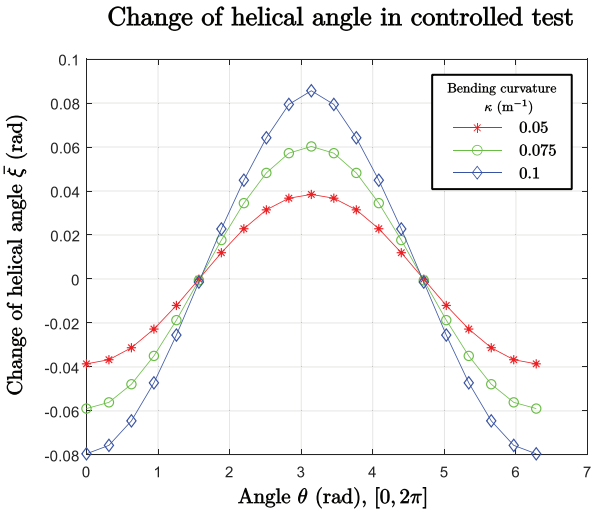

Fig. 17. Change of helical angle by controlling κ.

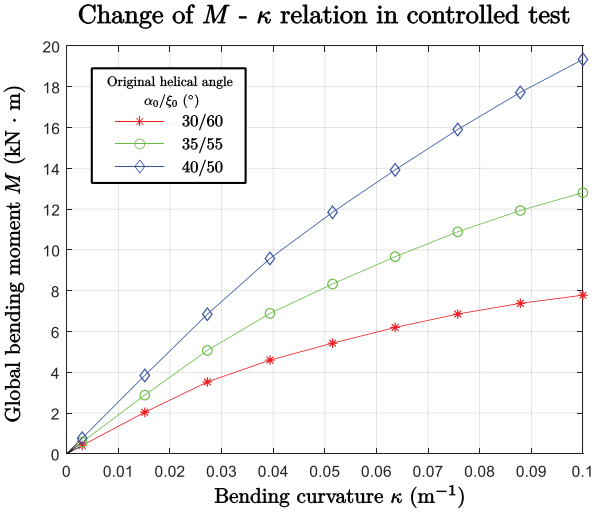

Fig. 18. Change of M - κ relation by controlling α_0/ξ_0.

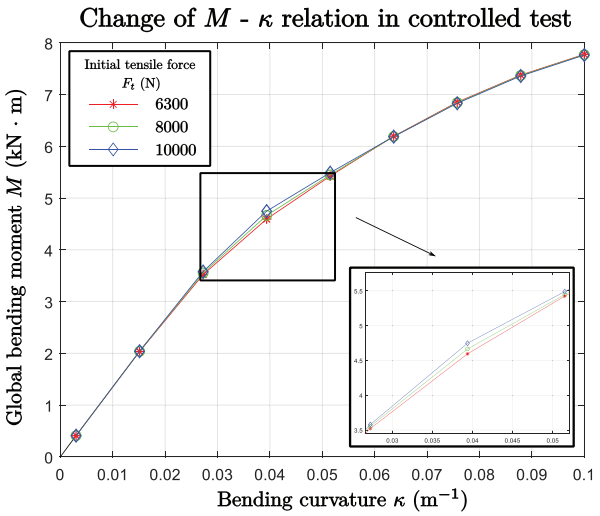

Fig. 19. Change of M - κ relation by controlling F_t.

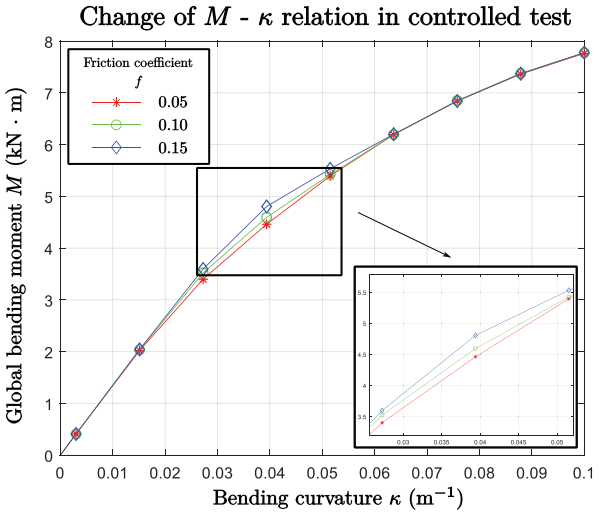

Fig. 20. Change of M - κ relation by controlling f.

If the helical angle variation is omitted, all curves would be linear. Only the change of original helical angle will act on the results of this parametric analysis.

The parametric results corresponding to original helical angle, initial tensile force and friction coefficient are presented in the following Figs. 18–20.

In Fig. 18, it can be apparently shown that the increasing of original helical angle exhibits a significant influence on the whole value of global bending moment with respect to bending curvature. It will require larger force and moment to bend the pipe while the original helical angle increases.

In contrast, differ from the results in Fig. 18–20 illustrate another similar ramification of the M - κ relation, which is, the final value of global bending moment does not change, while the local curve's shape slightly changes. This is mainly because the two parameters do not have influence on the variable helical angle corresponding to the end fitting of the flexible pipes, yet can show an effect on the local part of armour wires. If initial tensile force or friction coefficient increases, larger bending moment is in demand while under the same bending condition.

8. Conclusion

In this work a theoretical method for variable helical angle of tensile armour wires in bent flexible pipes is presented. On basis of differential geometrical discussion and mechanical model on curved beam theory, a system of non-linear differential equations is established to analyze the local behavior of armour wires in flexible pipes. The process of calculation is written in detail including a developed analytical discussion on armour wires' strain theory before and after wires' slip. Due to

complexity of the local differential geometrical behavior of armour wires, the changing of helical angle with respect to bending curvature is usually implicit in previous work. However, the study shows that the underlying mechanism of variable helical angle of armour wires in bent flexible pipes may influence the global bending process of flexible pipes, which will have a wide range of applications in further theoretical research in this filed.

Several case studies are made to investigate the reliability of this theoretical method. Throughout a comparison with a theoretical model in previous paper, the sound theory of local behavior in armour wires that accords with the strain discussion is substantiated. The calculation in the study shows that the slips and helical angle corresponding to bending all have sinusoidal shapes versus parametrical coordinate θ. In addition, by applying the variable helical angle theory into global bending model of flexible pipes, a nonlinear response in a monotonic loading of the bending moment-curvature relation is revealed theoretically. All the data and results can be a satisfactory reference to simulate the bending situation of tensile armour layers in flexible pipes. Controlled verification in global bending problem including every layers in flexible pipes is also implemented, as well as the parametric analysis corresponding to original helical angle, initial tensile force, friction coefficient and bending curvature which can reveal a series of conclusions based on the variable helical angle hypothesis. The provided results enable a preliminary examination of the global bending research which can be a reliable guidance for further cyclic study of bent flexible pipes.

Although the theoretical study presented in this paper finds evidence for predicting local behavior of armour wires in flexible pipes, due to its limitation some factors are still not satisfactory. The effect of variable helical angle in tensile armour wires on global bending is sensitive to the size of pipe. The cyclic bending study is also not included since it is convoluted to improve the non-linear differential system. Further studies are therefore in demand to consider the cyclic effect on this bending model of flexible pipes. The reliable prediction of global bending problem for multiple layers with the developed theoretical method is in need of investigation in the future.

Acknowledgments

The authors acknowledge the support from China National Key Research and Development Plan (Grant No. 2016YFC0303702), National Natural Science Foundation of China (Nos. 51904181 and 51809276) and National Council of Scientific and Technological Development (CNPq) (No. 302380/2013-2).

References

[1] J. Feret, C. Bournazel, Calculation of stresses and slip in structural layers of unbonded flexible pipes, J. Offshore Mech. Arct. Eng. 109 (3) (1987) 263–269.
[2] J. Out, B. Von Morgen, Slippage of helical reinforcing on a bent cylinder, Eng. Struct. 19 (6) (1997) 507–515.
[3] D. McIver, A method of modelling the detailed component and overall structural behaviour of flexible pipe sections, Eng. Struct. 17 (4) (1995) 254–266.
[4] G.A. Costello, Theory of Wire Rope, Springer Science & Business Media, 1997.
[5] J. Witz, Z. Tan, On the flexural structural behaviour of flexible pipes, umbilicals and marine cables, Mar. Struct. 5 (2) (1992) 229–249.
[6] S. Sævik, A finite element model for predicting stresses and slip in flexible pipe armouring tendons, Comput. Struct. 46 (2) (1993) 219–230.
[7] S. Sævik, S. Bruaseth, Theoretical and experimental studies of the axisymmetric behaviour of complex umbilical cross-sections, Appl. Ocean Res. 27 (2) (2005) 97–106.
[8] S. Sævik, Theoretical and experimental studies of stresses in flexible pipes, Comput. Struct. 89 (23) (2011) 2273–2291.
[9] S. Sævik, J. Gjøsteen, Strength analysis modelling of flexible umbilical members for marine structures, J. Appl. Math. 2012 (2012).
[10] J. Ferét, G. Momplot, Caflex – A Program for Capacity Analysis of Flexible Pipes, Theory Manual, SINTEF Report no.: STF(1992).
[11] J. Féret, J. Leroy, P. Estrier, Calculation of Stresses and Slips in Flexible Armor Layers with Layers Interaction, Technical Report, American Society of Mechanical Engineers, New York, NY (United States), 1995.
[12] J.-M. Leroy, P. Estrier, Calculation of stresses and slips in helical layers of dynamically bent flexible pipes, Oil Gas Sci. Technol. 56 (6) (2001) 545–554.
[13] R. Ramos, C.P. Pesce, A consistent analytical model to predict the structural behavior of flexible risers subjected to combined loads, J. Offshore Mech. Arct. Eng. 126 (2) (2004) 141–146.
[14] M. Brack, L.M. Troina, J.R.M. de Sousa, Flexible riser resistance against combined axial compression, bending, and torsion in ultra-deep water depths, in: Proceedings of the ASME 2005 24th International Conference on Offshore Mechanics and Arctic Engineering, American Society of Mechanical Engineers, 2005, pp. 821–829.
[15] A. Bahtui, H. Bahai, G. Alfano, A finite element analysis for unbonded flexible risers under axial tension, in: Proceedings of the ASME 2008 27th International Conference on Offshore Mechanics and Arctic Engineering, American Society of Mechanical Engineers, 2008, pp. 529–534.
[16] A. Bahtui, H. Bahai, G. Alfano, A finite element analysis for unbonded flexible risers under torsion, J. Offshore Mech. Arct. Eng. 130 (4) (2008) 041301.
[17] N.H. Østergaard, A. Lyckegaard, J.H. Andreasen, A method for prediction of the equilibrium state of a long and slender wire on a frictionless toroid applied for analysis of flexible pipe structures, Eng. Struct. 34 (2012) 391–399.
[18] N.H. Østergaard, A. Lyckegaard, J. Andreasen, Simulation of frictional effects in models for calculation of the equilibrium state of flexible pipe armouring wires in compression and bending, Raken. Mek. (J. Struct. Mech.) 44 (3) (2011) 243–259.
[19] M. Tang, C. Yang, J. Yan, Q. Yue, Validity and limitation of analytical models for the bending stress of a helical wire in unbonded flexible pipes, Appl. Ocean Res. 50 (2015) 58–68.
[20] M. Zhang, X. Chen, S. Fu, Y. Guo, L. Ma, Theoretical and numerical analysis of bending behavior of unbonded flexible risers, Mar. Struct. 44 (2015) 311–325.
[21] L. Dong, Y. Huang, G. Dong, Q. Zhang, G. Liu, Bending behavior modeling of unbonded flexible pipes considering tangential compliance of interlayer contact interfaces and shear deformations, Mar. Struct. 42 (2015) 154–174.
[22] L. Dong, S. Tu, Y. Huang, G. Dong, Q. Zhang, A model for the biaxial dynamic bending of unbonded flexible pipes, Mar. struct. 43 (2015) 125–137.
[23] C.M. Larsen, S. Sævik, J. Qvist, Design analysis, Technical Report, NTNU / 4Subsea / MARINTEK, Trondheim, Norway, 2014.
[24] Y. Bai, T. Liu, W. Ruan, W. Chen, Mechanical behavior of metallic strip flexible pipe subjected to tension, Compos. Struct. 170 (2017) 1–10.
[25] F. Cornacchia, T. Liu, Y. Bai, N. Fantuzzi, Tensile strength of the unbonded flexible pipes, Compos. Struct. 218 (2019) 142–151.
[26] Y. Zhou, M.A. Vaz, A quasi-linear method for frictional model in helical layers of bent flexible risers, Mar. Struct. 51 (2017) 152–173.
[27] E. Kebadze, I. Kraincanic, et al., Non-linear bending behaviour of offshore flexible pipes, in: Proceedings of the Ninth International Offshore and Polar Engineering Conference, International Society of Offshore and Polar Engineers, 1999.
[28] E. Kebadze, Theoretical Modelling of Unbonded Flexible Pipe Cross-sections., South Bank University, 2000 Ph.D. thesis.

[29] I. Kraincanic, E. Kebadze, Slip initiation and progression in helical armouring layers of unbonded flexible pipes and its effect on pipe bending behaviour, J. Strain Anal. Eng. Des. 36 (3) (2001) 265–275.
[30] J. Witz, A case study in the cross-section analysis of flexible risers, Mar. Struct. 9 (9) (1996) 885–904.
[31] M.P. Do Carmo, M.P. Do Carmo, Differential Geometry of Curves and Surfaces, 2, Prentice-hall Englewood Cliffs, 1976.
[32] J. Ericksen, C. Truesdell, Exact theory of stress and strain in rods and shells, Arch. Ration Mech. Anal. 1 (1) (1957) 295–323.
[33] E. Reissner, On finite deformations of space-curved beams, Z. Angew. Math. Phys. 32 (6) (1981) 734–744.
[34] A. Love, A Treatise on the Mathematical Theory of Elasticity, Dover, 1944.
[35] T. Dai, S. Sævik, N. Ye, Friction models for evaluating dynamic stresses in non-bonded flexible risers, Mar. Struct. 55 (2017) 137–161.